

Current Mode Control of Non-Isolated Multi-Phase Interleaved Buck-Boost Converter for Military Battery Charging Application

Ahmet Karaarslan

*Department of Electrical and Electronics Engineering
Ankara Yildirim Beyazit University
Ankara, Turkey
akaraarslan@gmail.com*

Ali Shaibu*

*Department of Electrical and Electronics Engineering
Ankara Yildirim Beyazit University
Ankara, Turkey
Shaibu.ali.imran@gmail.com*

Abstract— Power conversion devices are essential in a remote off-grid site, typically for military purposes where several types of equipment with varying input characteristics are supplied essentially by the same energy source, necessitating the use of a buck-boost converter for DC-DC applications. Because the conventional buck-boost converter's inverting output voltage is incompatible with some applications, the two-switch buck-boost converter is recommended for battery charging in military applications. The nominal input voltage range of the five-phase interleaved buck-boost converter is 9 – 36 V, the output voltage is 28 V, the output power is 3.3 kW, and the switching frequency is 100 kHz. The simulation of the converter with current mode control in the MATLAB/Simulink simulation environment was performed to confirm validity of the operational theory and the simulation results show consistency with theoretical values. Maximum of 74.41 ms and 51.35 % were recorded under all conditions of operation for the settling and overshoot respectively. The obtained data indicates a 1–2 % variation between the measured and theoretical duty cycle.

Keywords— *Buck-boost Converter, Current Mode Control, Interleaved Converter, PI Control, DC-DC Converter.*

I. INTRODUCTION

Power conversion devices are unavoidable in remote areas where access to the electrical grid is not possible. This, in turn, leads to massive research investments in high efficiency and high-power density energy storage systems and power conversion devices, particularly in military applications where equipment with varying input voltage requirements is powered by a single power storage unit, necessitating extremely high efficiency and reliability of power conversion devices. Electronic and communication equipment used in the military, such as Land Mobile Radios (LMRs), night vision cameras, and naval communication systems, rely heavily on batteries. Batteries are also used in the fields of avionics and military vehicles. On a battlefield, the risk of a soldier losing his life as a result of an inadequately charged battery is significantly higher [1,2]. As a result, reliable, high-power-density, efficient, and fast charging converters are required. With the development of power electronics and

control theory and formulation, a wide range of voltage and current characteristics can be designed and achieved to meet the requirements of the equipment being operated or to obtain a suitable charging profile for specific battery chemistry being charged.

To maximize the use of energy in off-grid applications, such as some military operations, very efficient, reliable, and robust converters are required [3,4]. As a result, massive research and investments have been made in the field of power converters, resulting in the improvement and discovery of more effective algorithms and techniques used to achieve a much better operation. Converters are essential to the operations of most military devices and hence the need to further investigate and improve existing converter topologies and or algorithms used in their control.

The switched-mode power supply (SMPS) has become an integral part of most household appliances and industrial equipment [5]. The principle of operation of the SMPS relies on the energy storage capabilities of some passive elements such as in the magnetic field of the inductor and also the electric field of the capacitor in conjunction with electronic switching devices such as the MOSFET and IGBTs present the ability to control the energy flow in and out of the storage element with the desired voltage and current characteristics to the load [6]. The SMPS has the advantage of high efficiency compared to other power conversion methods such as the linear regulator.

Unlike the linear regulators, the switching regulators convert a direct current (DC) source from one voltage level to another by momentarily storing the input energy and then releasing it to the output at a different voltage [7-9]. The energy is stored in the magnetic field of inductors or transformers, and also can be stored in the electric field of capacitors. The amount of energy transferred from the input to output is a function of the applied frequency and duty cycle to a particular DC-DC converter topology, hence the input current, output current, output voltage and power can be controlled effectively.

This paper seeks to investigate wide input voltage of 6 – 36 V, 3.3 kW and with 28 VDC as per the MIL-STD-1275E DC-DC converter for military application utilization multiphase interleaved buck-boost converter due to the power demand of the military equipment. Several converters are proposed for military application. (Alarabi & Karaarslan, 2020) proposed an isolated multiphase interleaved converter for military battery charging, consisting of a four phase interleaved boost converter, a full bridge converter for DC-AC conversion, a transformer, and the final rectification stage. The main disadvantage of the proposed converter was the number of components and the level of voltage transformation required to achieve the desired output voltage. Additionally, the presence of an isolation transformer adds more weight and space occupied by the converter. (Aktas, 2020) Ali also demonstrated a battery charging method for military battery charging applications that makes use of a charging circuit that includes an initial rectification, PFC boost, full-bridge, and push-pull converter stages. Although the conversion is achieved, the complexity of the control circuit and component count is a major disadvantage for implementation. As a result, the five phase non-isolated interleaved buck-boost converter is investigated in this paper due to its simplicity of implementation and reduced component count, which reduces switching losses.

II. METHODS

The proposed converter is based on the non-inverting buck-boost converter topology. The proposed interleaved converter has five buck-boost converters connected in parallel as depicted in Fig. 1. The converter is designed to meet an input voltage range of 9 – 36 V, an output voltage of 28 V and an output power of 3.3 kW. The inductors $L1$, $L2$, $L3$, $L4$ and $L5$ of equal inductances are designed to operate in continuous conduction mode, implying that the inductor current never reaches zero for the entire period of operation.

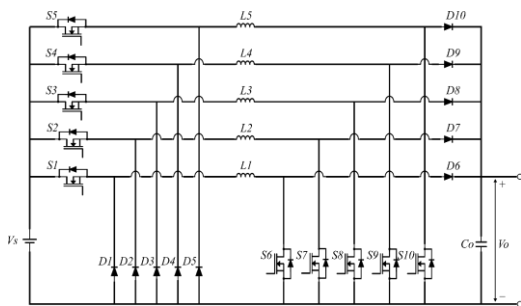


Fig. 1. Five phase interleaved buck-boost converter.

Due to the interleaved operation of the proposed design, the current is shared equally among the inductors as depicted in Fig. 2, thereby reducing the size of the conductor and magnetic core required relative to a single leg converter of the same ratings. The current ripple is further reduced and also the output voltage ripple is reduced since the output capacitor is constantly supplied in all modes of operation. The converter operation is characterized by ten distinct modes of operation as described below.

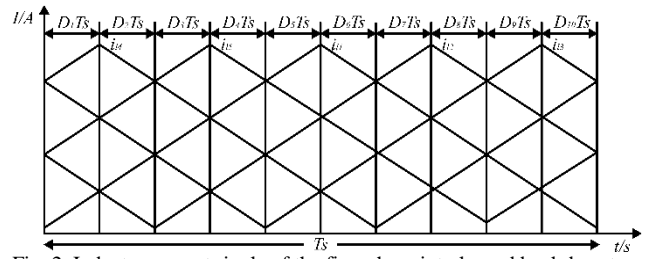


Fig. 2. Inductor current ripple of the five-phase interleaved buck-boost converter

Mode 1

Fig. 3 depicts the conduction path of the converter for the period $0 < t < DTs$. In this mode of operation switches $S1$, $S4$, $S5$, $S6$, $S9$ and $S10$ are in the conduction mode, therefore energy is being stored in the magnetic field of inductors $L1$, $L4$ and $L5$. Diodes $D2$, $D3$, $D7$ and $D8$ are also conducting, supplying the load and output capacitor.

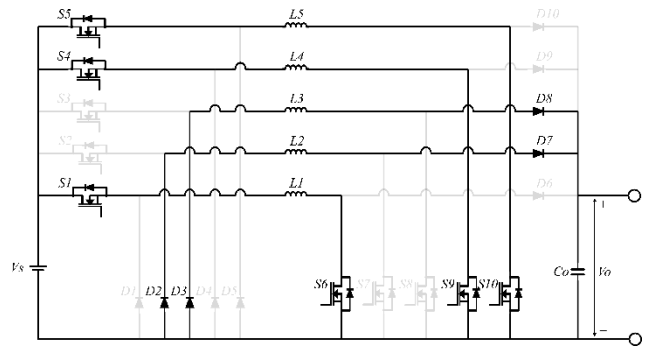


Fig. 3. Equivalent circuit of mode 1

This mode of operation is expressed in (1) as follows:

$$\left. \begin{aligned} \frac{di_{L1}}{dt} &= \frac{V_S}{L_1}; & \frac{di_{L2}}{dt} &= \frac{-V_O}{L_2}; & \frac{di_{L3}}{dt} &= \frac{-V_O}{L_2}; \\ \frac{di_{L4}}{dt} &= \frac{V_S}{L_4}; & \frac{di_{L5}}{dt} &= \frac{V_S}{L_5}; \\ \frac{Cdv_O}{dt} &= i_{L2} + i_{L3} - I_O \end{aligned} \right\} \quad (1)$$

Mode 2

Fig. 4 depicts the conduction path of the converter for the period $DTs < t < D2Ts$. In this mode of operation switches $S1$, $S5$, $S6$ and $S10$ are in the conduction mode, therefore energy is being stored in the magnetic field of inductors $L1$ and $L5$. Diodes $D2$, $D3$, $D4$, $D7$, $D8$ and $D9$ are also conducting, supplying the load and output capacitor.

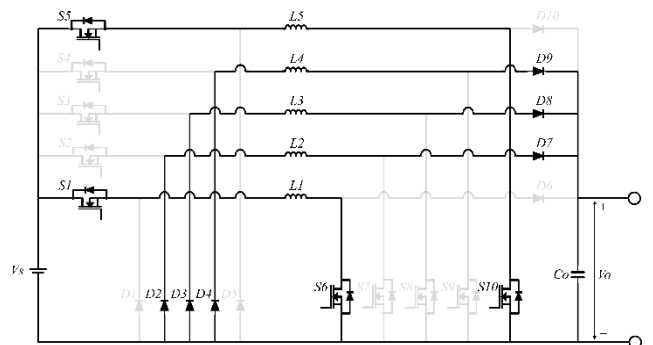


Fig. 4. Equivalent circuit of mode 2

This mode of operation is expressed in (2) as follows:

$$\left. \begin{aligned} \frac{di_{L1}}{dt} &= \frac{V_S}{L_1}; \quad \frac{di_{L2}}{dt} = \frac{-V_O}{L_2}; \quad \frac{di_{L3}}{dt} = \frac{-V_O}{L_3}; \\ \frac{di_{L4}}{dt} &= \frac{-V_O}{L_4}; \quad \frac{di_{L5}}{dt} = \frac{V_S}{L_5}; \\ \frac{Cdv_o}{dt} &= i_{L2} + i_{L3} + i_{L4} - I_O \end{aligned} \right\} \quad (2)$$

$$\left. \begin{aligned} \frac{di_{L1}}{dt} &= \frac{V_S}{L_1}; \quad \frac{di_{L2}}{dt} = \frac{V_S}{L_2}; \quad \frac{di_{L3}}{dt} = \frac{-V_O}{L_3}; \\ \frac{di_{L4}}{dt} &= \frac{-V_O}{L_4}; \quad \frac{di_{L5}}{dt} = \frac{-V_O}{L_5}; \\ \frac{Cdv_o}{dt} &= i_{L3} + i_{L4} + i_{L5} - I_O \end{aligned} \right\} \quad (4)$$

Mode 3

Fig. 5 depicts the conduction path of the converter for the period $D2Ts < t < D3Ts$. In this mode of operation switches $S1, S2, S5, S6, S7$ and $S10$ are in the conduction mode, therefore energy is being stored in the magnetic field of inductors $L1, L2$ and $L5$. Diodes $D3, D4, D8$ and $D9$ are also conducting, supplying the load and output capacitor.

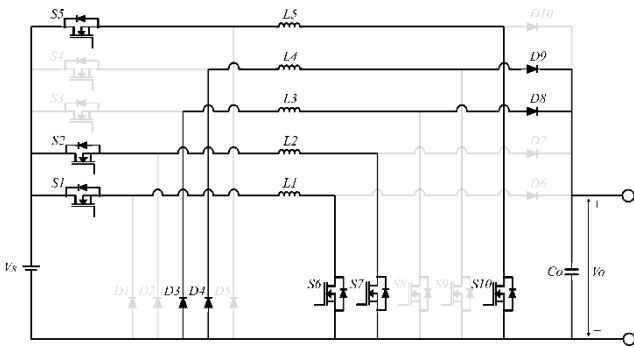


Fig. 5. Equivalent circuit of mode 3

This mode of operation is expressed in (3) as follows:

$$\left. \begin{aligned} \frac{di_{L1}}{dt} &= \frac{V_S}{L_1}; \quad \frac{di_{L2}}{dt} = \frac{V_S}{L_2}; \quad \frac{di_{L3}}{dt} = \frac{-V_O}{L_3}; \\ \frac{di_{L4}}{dt} &= \frac{-V_O}{L_4}; \quad \frac{di_{L5}}{dt} = \frac{V_S}{L_5}; \\ \frac{Cdv_o}{dt} &= i_{L3} + i_{L4} - I_O \end{aligned} \right\} \quad (3)$$

Mode 5

Fig. 7 depicts the conduction path of the converter for the period $D4Ts < t < D5Ts$. In this mode of operation switches $S1, S2, S3, S6, S7$ and $S8$ are in the conduction mode, therefore energy is being stored in the magnetic field of inductors $L1, L2$ and $L3$. Diodes $D4, D5, D9$ and $D10$ are also conducting, supplying the load and output capacitor.

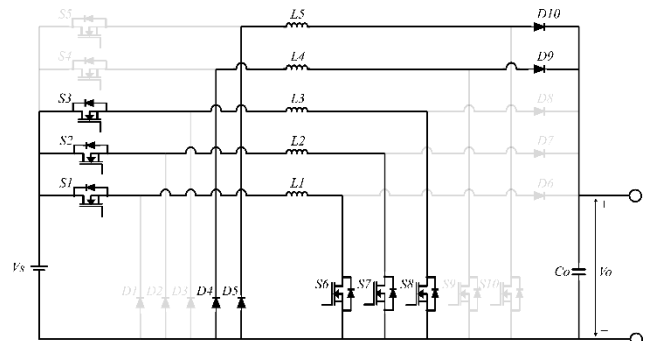


Fig. 7. Equivalent circuit of mode 5

This mode of operation is expressed in (5) as follows:

$$\left. \begin{aligned} \frac{di_{L1}}{dt} &= \frac{V_S}{L_1}; \quad \frac{di_{L2}}{dt} = \frac{V_S}{L_2}; \quad \frac{di_{L3}}{dt} = \frac{V_S}{L_3}; \\ \frac{di_{L4}}{dt} &= \frac{-V_O}{L_4}; \quad \frac{di_{L5}}{dt} = \frac{-V_O}{L_5}; \\ \frac{Cdv_o}{dt} &= i_{L4} + i_{L5} - I_O \end{aligned} \right\} \quad (5)$$

Mode 4

Fig. 6 depicts the conduction path of the converter for the period $D3Ts < t < D4Ts$. In this mode of operation switches $S1, S2, S6,$ and $S7$ are in the conduction mode, therefore energy is being stored in the magnetic field of inductors $L1$ and $L2$. Diodes $D3, D4, D5, D8, D9$ and $D10$ are also conducting, supplying the load and output capacitor.

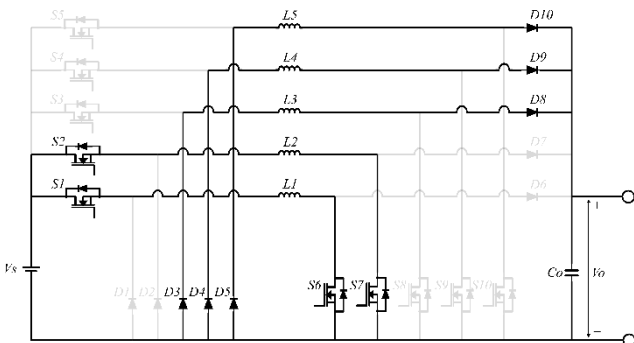


Fig. 6. Equivalent circuit of mode 4

This mode of operation is expressed in (4) as follows:

Mode 6

Fig. 8 depicts the conduction path of the converter for the period $D5Ts < t < D6Ts$. In this mode of operation switches $S2, S3, S7$ and $S8$ are in the conduction mode, therefore energy is being stored in the magnetic field of inductors $L2$ and $L3$. Diodes $D1, D4, D5, D6, D9$ and $D10$ are also conducting, supplying the load and output capacitor.

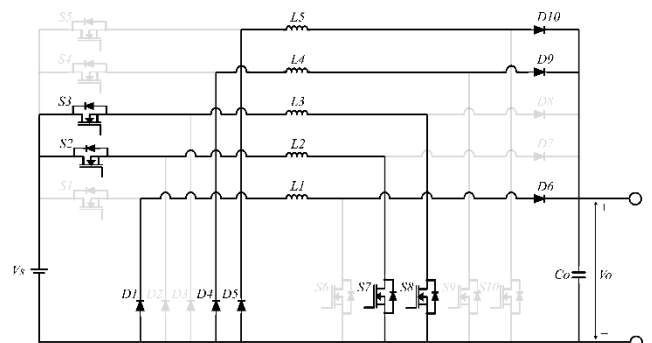


Fig. 8. Equivalent circuit of mode 6

This mode of operation is expressed in (6) as follows:

$$\left. \begin{aligned} \frac{di_{L1}}{dt} &= \frac{-V_O}{L_1}; & \frac{di_{L2}}{dt} &= \frac{V_S}{L_2}; & \frac{di_{L3}}{dt} &= \frac{V_S}{L_2}; \\ \frac{di_{L4}}{dt} &= \frac{-V_O}{L_4}; & \frac{di_{L5}}{dt} &= \frac{-V_O}{L_5}; \\ \frac{Cdv_o}{dt} &= i_{L1} + i_{L4} + i_{L5} - I_O \end{aligned} \right\} \quad (6)$$

$$\left. \begin{aligned} \frac{di_{L1}}{dt} &= \frac{-V_O}{L_1}; & \frac{di_{L2}}{dt} &= \frac{-V_O}{L_2}; & \frac{di_{L3}}{dt} &= \frac{V_S}{L_2}; \\ \frac{di_{L4}}{dt} &= \frac{V_S}{L_4}; & \frac{di_{L5}}{dt} &= \frac{-V_O}{L_5}; \\ \frac{Cdv_o}{dt} &= i_{L1} + i_{L3} + i_{L5} - I_O \end{aligned} \right\} \quad (8)$$

Mode 7

Fig. 9 depicts the conduction path of the converter for the period $D6Ts < t < D7Ts$. In this mode of operation switches $S2, S3, S4, S7, S8$ and $S9$ are in the conduction mode, therefore energy is being stored in the magnetic field of inductors $L2, L3$ and $L4$. Diodes $D1, D5, D6$ and $D10$ are also conducting, supplying the load and output capacitor.

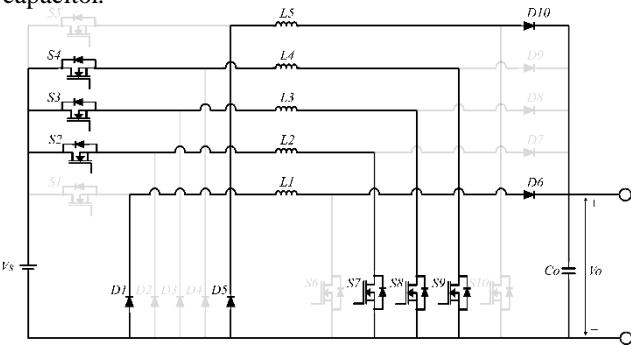


Fig. 9. Equivalent circuit of mode 7

This mode of operation is expressed in (7) as follows:

$$\left. \begin{aligned} \frac{di_{L1}}{dt} &= \frac{-V_O}{L_1}; & \frac{di_{L2}}{dt} &= \frac{V_S}{L_2}; & \frac{di_{L3}}{dt} &= \frac{V_S}{L_2}; \\ \frac{di_{L4}}{dt} &= \frac{V_S}{L_4}; & \frac{di_{L5}}{dt} &= \frac{-V_O}{L_5}; \\ \frac{Cdv_o}{dt} &= i_{L1} + i_{L5} - I_O \end{aligned} \right\} \quad (7)$$

Mode 8

Fig. 10 depicts the conduction path of the converter for the period $D7Ts < t < D8Ts$. In this mode of operation switches $S3, S4, S8$ and $S9$ are in the conduction mode, therefore energy is being stored in the magnetic field of inductors $L3$ and $L4$. Diodes $D1, D2, D5, D6, D7$ and $D10$ are also conducting, supplying the load and output capacitor.

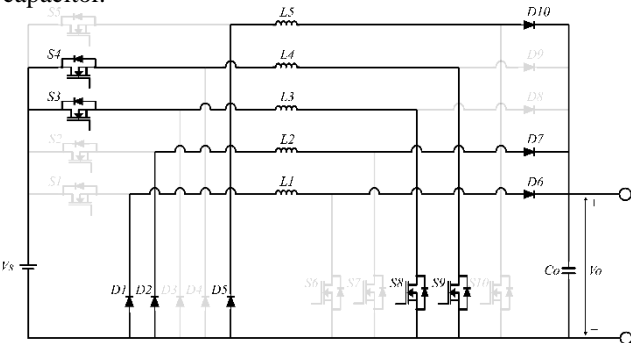


Fig. 10. Equivalent circuit of mode 8

This mode of operation is expressed in (8) as follows:

Mode 9

Fig. 11 depicts the conduction path of the converter for the period $D9Ts < t < D10Ts$. In this mode of operation switches $S3, S4, S5, S8, S9$ and $S10$ are in the conduction mode, therefore energy is being stored in the magnetic field of inductors $L3, L4$ and $L5$. Diodes $D1, D2, D6,$ and $D7$ are also conducting, supplying the load and output capacitor.

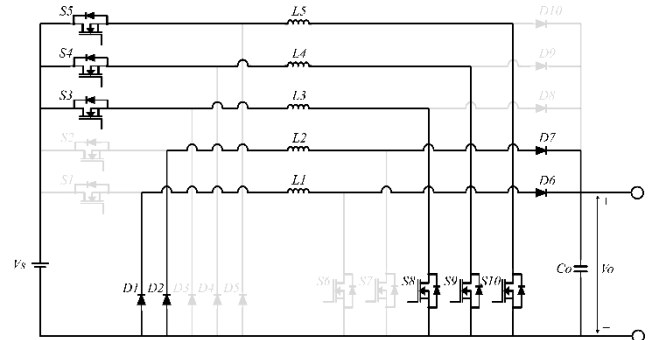


Fig. 11. Equivalent circuit of mode 9

This mode of operation is expressed in (9) as follows:

$$\left. \begin{aligned} \frac{di_{L1}}{dt} &= \frac{-V_O}{L_1}; & \frac{di_{L2}}{dt} &= \frac{-V_O}{L_2}; & \frac{di_{L3}}{dt} &= \frac{V_S}{L_2}; \\ \frac{di_{L4}}{dt} &= \frac{V_S}{L_4}; & \frac{di_{L5}}{dt} &= \frac{V_S}{L_5}; \\ \frac{Cdv_o}{dt} &= i_{L1} + i_{L2} - I_O \end{aligned} \right\} \quad (9)$$

Mode 10

Fig. 12 depicts the conduction path of the converter for the period $D8Ts < t < D9Ts$. In this mode of operation switches $S4, S5, S9$ and $S10$ are in the conduction mode, therefore energy is being stored in the magnetic field of inductors $L4$ and $L5$. Diodes $D1, D2, D3, D6, D7$ and $D8$ are also conducting, supplying the load and output capacitor.

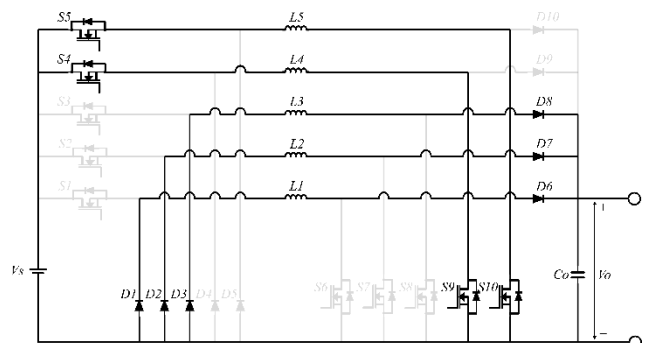


Fig. 12. Equivalent circuit of mode 10

The equations describing this mode of operation are expressed as follows:

$$\left. \begin{aligned} \frac{di_{L1}}{dt} &= \frac{-V_O}{L_1}; \quad \frac{di_{L2}}{dt} = \frac{-V_O}{L_2}; \quad \frac{di_{L3}}{dt} = \frac{-V_O}{L_3}; \\ \frac{di_{L4}}{dt} &= \frac{V_S}{L_4}; \quad \frac{di_{L5}}{dt} = \frac{V_S}{L_5}; \\ \frac{Cdv_o}{dt} &= i_{L1} + i_{L2} + i_{L3} - I_O \end{aligned} \right\} \quad (10)$$

Under steady-state operation conditions, the characteristic equations defining this mode of operation of a single leg of the converter are given in the series of equations below and since each leg of the converter is of equal characteristic hence equal parameters required for the optimal operation of the converter. Considering leg 1 of the converter over the entire period of operation, when switches $S1$ and $S6$ are conducting as depicted in mode 1, the steady-state inductor voltage v_L is the same as the source voltages V_S , as presented in (11) and (12) expresses the inductor ripple current.

$$v_L = V_S = L \frac{di_L}{dt} \quad (11)$$

$$\Delta i_{L_closed} = \left(\frac{V_S}{L}\right) DT_s \quad (12)$$

When switch $S1$ and $S6$ are not conducting as depicted in mode 6, the steady-state inductor voltage v_L is the same as the output voltage V_O , as presented in (13) and (14) expresses the inductor ripple current.

$$v_{L1} = -V_O = L \frac{di_L}{dt} \quad (13)$$

$$\Delta i_{L_open} = \left(\frac{-V_O}{L}\right) (1-D)T_s \quad (14)$$

Under steady-state operation conditions, the net change in inductor current over a period of operation should sum up to zero as expressed in (15).

$$\left. \begin{aligned} \Delta i_{L_closed} + \Delta i_{L_open} &= 0 \\ \left(\frac{V_S}{L}\right) DT_s + \left(\frac{-V_O}{L}\right) (1-D)T_s &= 0 \end{aligned} \right\} \quad (15)$$

The input and output voltage relationship is expressed in (16) after simplifying the terms in (15).

$$V_O = \frac{DV_S}{1-D} \quad (16)$$

The average input power must be equal to the average output power through the load in a steady-state operation as expressed in equations below.

Average output power:

$$P_o = \frac{V_o^2}{R} = V_o I_o \quad (17)$$

Average input power:

$$V_S I_S = V_S \times 5I_L \times D \quad (18)$$

Average input power = Average output power. Average inductor current per phase expressed by I_L .

$$\left. \begin{aligned} V_S \times 5I_L \times D &= \frac{V_o^2}{R} \\ V_S \times 5I_L \times D &= \frac{V_S^2 D^2}{(1-D)^2 R} \\ I_L &= \frac{V_S D}{5(1-D)^2 R} \end{aligned} \right\} \quad (19)$$

The maximum inductor current is simplified in (20) below.

$$\left. \begin{aligned} I_{max} &= I_L + \frac{\Delta i_L}{2} \\ I_{max} &= \frac{V_S D}{5(1-D)^2 R} + \frac{V_S D}{2Lf_s} \end{aligned} \right\} \quad (20)$$

Where:

$$f_s = \frac{1}{T_s} \quad (21)$$

The minimum inductor current is simplified in (22) below.

$$\left. \begin{aligned} I_{min} &= I_L - \frac{\Delta i_L}{2} \\ I_{min} &= \frac{V_S D}{5(1-D)^2 R} - \frac{V_S D}{2Lf_s} \end{aligned} \right\} \quad (22)$$

The inductance value for a certain desired level of current ripple is expressed in (22).

$$L_1 = L_2 = L_3 = L_4 = L_5 = \frac{DV_S}{\Delta i_L f_s} \quad (23)$$

I_{min} must be larger than or equal to zero in order to continue operating in continuous conduction mode. This indicates that there is a minimum value of inductance L_{min} required to operate in this state, which is given in (24).

$$L_{min} = \frac{5(1-D)^2 R}{2f_s} \quad (24)$$

The relationship between the required output capacitance and the output voltage ripple is expressed in (25):

$$\left. \begin{aligned} \frac{\Delta V_o}{V_o} &= \frac{D}{RC_o f_s} \\ C_o &= \frac{DV_o}{R\Delta V_o f_s} \end{aligned} \right\} \quad (25)$$

III. CONTROL METHOD

The control method uses a proportional integral (PI) controller for controlling the dynamic response of the proposed converter to achieve the desired output characteristics for a variation of load and or input voltage fluctuations. For the implementation of this control method on the proposed converter the negative feedback [10], the generated error as a result of the difference between the measured and reference value is passed through the PI controller and the effective duty signal required for the measured to reach the reference is generated. The generated duty signal is compared to a

sawtooth signal of constant frequency to generate the required switching frequency at the required duty cycle to facilitate a change in output voltage to reach the reference value.

Each unit of the multiphase converter operates in the same way as a single leg converter. Ideally, components of equal rating are used in each unit, resulting in them being identical. As a result, the same PWM signal with the same frequency and duty cycle can be used to drive each leg, however, the signals are phase-shifted by an angle θ , as shown in (26) [11,12].

$$\theta = \frac{360}{N} \quad (26)$$

Where:

θ = the phase difference between legs

N = number of legs

For a five-phase interleaved converter, all switching devices are controlled by the same control loop, however, the switch frequencies are phase-shifted by 72° ($360/5$) from their adjacent branch circuits resulting in successive switching of the switch pairs of $S1$ and $S6$, $S2$ and $S7$, $S3$ and $S8$, $S4$ and $S9$ and also $S5$ and $S10$.

The current mode control has two feedback loops: an external voltage feedback loop and an internal current feedback loop as shown in Fig. 13. The outer loop comprises the voltage loop, which measures and compares the output voltage to a fixed reference voltage [13-15] The difference generates an error signal for the outer loop PI controller to generate the reference current for the inner loop of the control. The inner loop comprises five distinct current loops with a PI controller for each of the loops. The reference current generated from the outer loop is compared to each inductor current, the difference between the reference and inductor current generates the current error [16,17]. Each PI controller in the inner loop generates the duty signal from the generated current error.

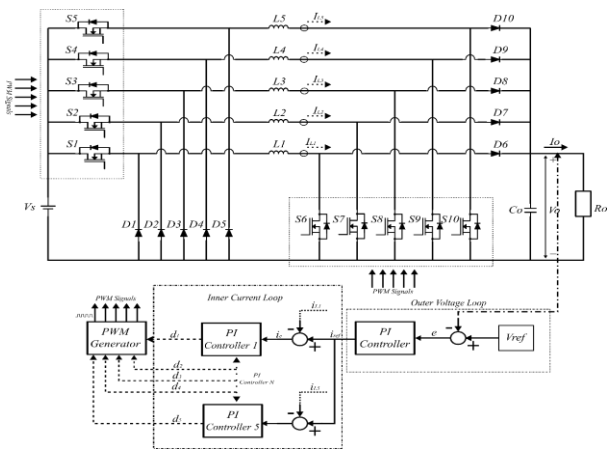


Fig. 13. Dual loop current mode PI control with each inductor current.

The outer loop is governed by (27) and (28):

$$v_e(t) = V_{ref}(t) - V_o(t) \quad (27)$$

Where $V_e(t)$, $V_{ref}(t)$ and $V_o(t)$ indicate the instantaneous error signal, reference and output voltages respectively.

$$i_{ref}(t) = v_e(t) \left(K_p + K_i \frac{1}{s} \right) \quad (28)$$

Where $i_{ref}(t)$, K_p and K_i indicates the reference current, proportional gain and integral gain of the outer loop respectively. The inner loop is governed by (29) and (30):

$$i_{en}(t) = i_{ref}(t) - i_{Ln}(t) \quad (29)$$

Where $i_{en}(t)$, $i_{ref}(t)$ and $i_{Ln}(t)$ indicate the nth current error, current reference and inductor currents respectively.

$$d_n(t) = i_{en}(t) \left(K_{pn} + K_{in} \frac{1}{s} \right) \quad (30)$$

Where $d_n(t)$, K_{p_n} and K_{i_n} indicates the duty signal, proportional gain and integral gain of each inner loop respectively.

IV. SIMULATION RESULTS

The equivalent model of the converter is simulated in the MATLAB/Simulink environment using the design parameters in Table I, and the results are provided in this section. Because the theoretical values and simulation results are congruent, the simulation shows the viability of the suggested converter and control mechanism.

TABLE I. SIMULATION PARAMETERS.

Parameter	Value
Input Voltage, V_{in}	9 – 36 V
Output Voltage, V_o	28 V
Output Power, P_o	3.3 kW
Output Current, I_o	117.86 A
Switching Frequency, f_s	100 kHz
Current Ripple	15% of I_L
Voltage Ripple	5% of V_o
Inductance, L	25 μ H
Minimum Inductance, L_{min}	1.88 μ H
Output Capacitor, C_o	650 μ F
Duty Cycle Range	43.8 – 75.7%

The current mode controlled interleaved buck-boost converter's output voltage response is simulated by varying the input voltage parameters within the converter's operating input voltage range. As can be seen in Fig. 14, the response observed for a voltage variation from 9 V to 36 V with an increment of 3 V per step. The output and inductor currents are shown in Fig. 15.

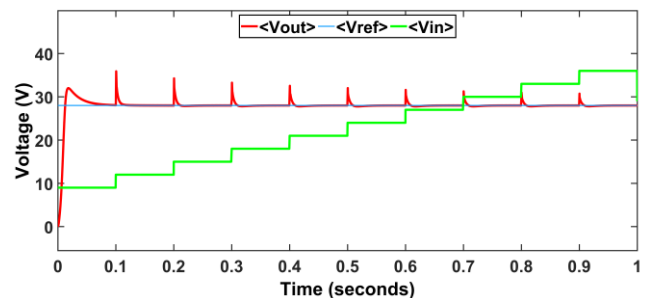


Fig. 14. Output voltage for varying input voltage.

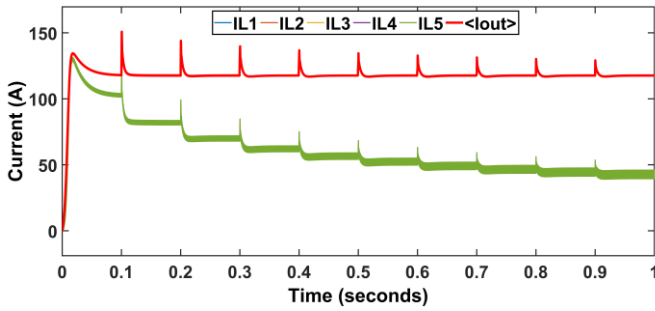


Fig. 15. Output and inductor current response with varying input voltage.

Fig. 16 shows the controller output as a result of changing input voltage, with the duty cycle decreasing as the input voltage increases.

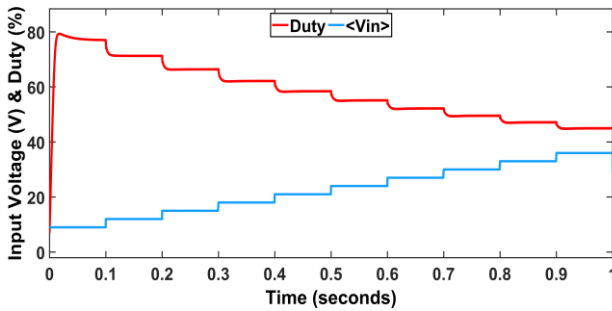


Fig. 16. Controller response for varying input voltage.

The output voltage and inductor current ripples are presented in Fig. 17 and Fig. 18 respectively. The inductor ripple shows the interleaving inductor currents phase-shifted from 72° from each other.

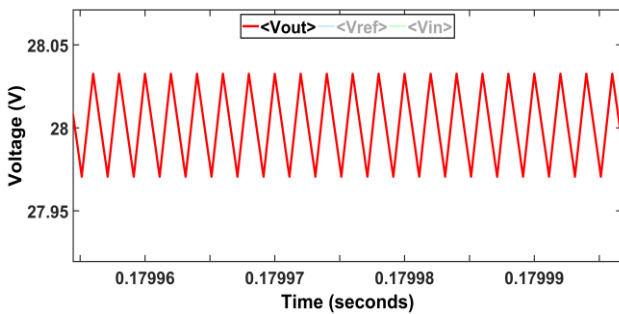


Fig. 17. Output voltage ripple.

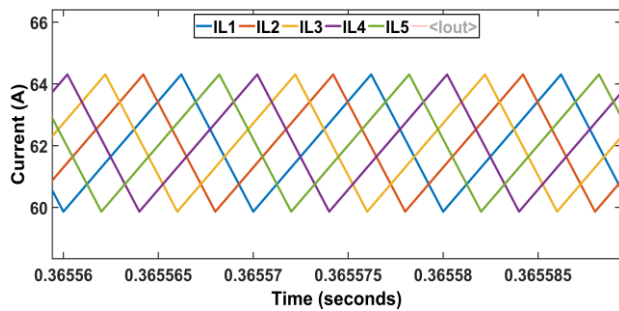


Fig. 18. Interleaved inductor current ripples.

Fig. 19 depicts the converter's output voltage. By varying the system's reference signal at a constant switching frequency and input voltage value, the output voltage

response is observed. For a nominal voltage of 28 V, the controller's response to a 10 V sudden increase in nominal voltage and a 10 V sudden decrease in nominal reference voltage.

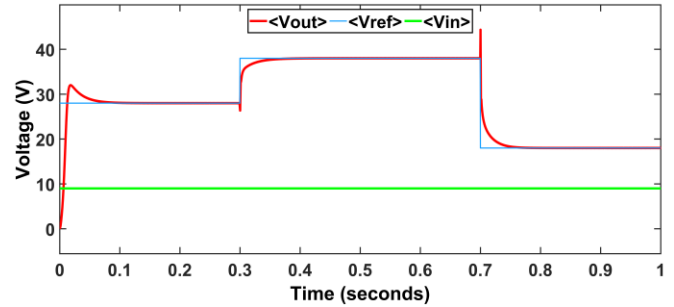


Fig. 19. Output voltage with varying reference voltage.

Fig. 20 depicts converter's output current. The output load response is investigated by varying the system's output load while maintaining a constant switching frequency, reference, and input voltage value. The observed response for an output load variation of +50/-50 % of the nominal output current.

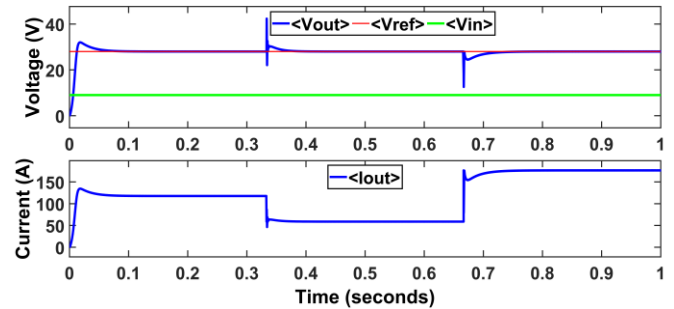


Fig. 20. Converter response for varying load.

Table II summarizes the observed performance characteristics from simulation results, including settling time, overshoots, measured and theoretical duty values for input voltage, reference voltage, and load variations. The maximum recorded settling time for the initial start-up of the converter was 74.41 ms under all conditions, however, after reaching steady-state, the maximum was 49.86 ms for reference voltage change from 28 V to 38 V and the minimum is 3.36 ms for load variation from 58.93 A to 176.79 A. The maximum overshoot is 51.35 % when the load varies between 117.86 A and 58.93 A, and the minimum is 9.85 % when the input voltage varies between 33 V and 36 V. The obtained data show a 1–2 % difference between the measured and theoretical duty cycle.

V. CONCLUSION

This paper presents a Simulink model and analyses a 28 V, 3.3 kW interleaved five-phase buck-boost converter for a military battery charging application. The equivalent MATLAB/Simulink model with the applied current mode control using each inductor current for the inner loop of the controller. The simulation results show consistency with the theoretical values indicating the validity of the model. Furthermore, the converter response under varying

conditions of operation were observed using the current mode control based feedback system to effectively control the output voltage to a level of steady state under conditions of varying input voltage range of 9 – 36 V, reference voltage variation for 50 % increment and decrement from the nominal 28 V to observe the robustness also the output load is varied under steady state conditions to observe the stability. The simulation results indicate as summarized in Table II indicates maximum

settling time of 74.41 ms and maximum overshoot of 27.07 % .

TABLE II. CONTROLLER RESPONSE CHARACTERISTICS.

Conditions		Control Response			
		Settling Time	Over/Undershoot	Measured Duty	Calculated Duty
Input Voltage Variation	9 – 12 V	11.32 ms	27.07%	71.32%	70.00%
	12 – 15 V	10.20 ms	21.29%	66.37%	65.12%
	15 – 18 V	8.87 ms	18.71%	62.12%	60.87%
	18 – 21 V	8.24 ms	16.32%	58.44%	57.14%
	21 – 24 V	7.93 ms	14.25%	55.20%	53.85%
	24 – 27 V	7.27 ms	12.71%	52.20%	50.91%
	27 – 30 V	7.14 ms	11.39%	49.54%	48.28%
	30 – 33 V	7.24 ms	10.61%	47.17%	45.90%
Reference Voltage Variation	33 – 36 V	6.63 ms	9.85%	44.94%	43.75%
	28 V	74.41 ms	14.21%	77.04%	75.65%
	38 V	49.86 ms	-6.21%	82.05%	80.85%
Output Load Variation	18 V	48.27 ms	18.18%	68.55%	66.67%
	117.86 A	74.41 ms	14.21%	77.04%	75.65%
	58.93 A	3.65 ms	51.35%	76.77%	75.65%
	176.79 A	3.36 ms	-55.79%	77.29%	75.65%
	28 V/117.86 A	74.41 ms	14.21%	77.04%	75.65%

REFERENCES

- [1] Chaari, M. Z., Al-Rahimi, R., (2021), The impact of wireless power charging on the future of the battlefield, 2021 International Wireless Communications and Mobile Computing (IWCMC), pp. 1563-1568.
- [2] Nxumalo, Z. C., Tarwireyi, P., Adigun, M. O., (2015), Lithium-based batteries in tactical military applications: A review, 2015 International Conference on Computer, Communications, and Control Technology (I4CT), pp. 575-579.
- [3] Frączek M, Górski K, Wolaniuk L., (2022), Possibilities of powering military equipment based on renewable energy sources, Applied Sciences, 12(2): 843-854.
- [4] G. F. Laghari, A. Umar and S. Abdullah, (2015) "Comparative analysis of multi-input DC/DC converter topology for hybrid renewable energy systems,"2015 Power Generation System and Renewable Energy Technologies (PGSRET), pp. 1-5.
- [5] Padhyay, S. B., Panda, G. K., Pradip, S. K., Das, S., (2015). Advance control techniques for DC/DC buck converter with improved performance. International Journal of Advanced Research in Electrical, Electronics and Instrumentation Engineering, 4: 201-208.
- [6] Kamil, M., (2007), Switch mode power supply (SMPS) topologies (part I), Microchip AN1114. Part I, pp. 1–48.
- [7] Farzin A. Sawai P. Kei E., Ngo L. T., Dorf, R. C., (2018), Modeling uncertainties in DC-DC converters with MATLAB and PLECS, Morgan & Claypool.
- [8] Sakka, M. A., Mierlo, J. V., Gualous, H., (2011), DC/DC converters for electric vehicles, Electric Vehicles - Modelling and Simulations. London, United Kingdom: IntechOpen.
- [9] Galm, J. M., (2003), Analysis and Opinion on the Operation of Switch Mode Power Supplies under Switched Voltage Phase Conditions, LayerZero Power Systems, Inc., pp. 1–8.
- [10] Ellabban, O., Mierlo, V. J.,(2009), Comparative evaluation of PID voltage mode, PI current mode, fuzzy and pwm based sliding mode control for dc-dc converters, The thirteen international middle-east power systems conference MEPCON'2009. pp. N/A.
- [11] Florides, M., (2010) Interleaved switching of dc/dc converters, University of Newcastle Upon Tyne, 68 pp.
- [12] Chang Y-N, Cheng H-L, Yen H-C, Chang C-H, Huang W-D., (2020) An interleaved dc/dc converter with soft-switching characteristic and high step-up ratio, Applied Sciences. 10(6), pp. 1-12.
- [13] Zhang, H. J., (2015), Modeling and loop compensation design of switching mode power supplies, Linear Technology, Vol. AN149fa, pp. 1–22.
- [14] Robert S., (2007), Understanding and applying current-mode control theory, Texas instruments SNVA555, pp. 1–26.
- [15] Jang, J., Pidaparthi, S. K., Choi, B., (2015), "Current mode control for LLC series resonant DC-to-DC converters," Energies, 8(6): 6098–6113.
- [16] Anon., (2006), Voltage Mode Control: The Modulator in Continuous Current Mode (CCM) of operation, Sipex Corporation Application Note 15, 10 pp.
- [17] Verma, S., Singh, S. K., Rao, A. G., (2013), Overview of control techniques for dc-dc converters, Research Journal of Engineering Sciences, 2(8): 18–21.